ACTA CHEMICA IASI, **17**, 137-150 (2009)

Nonlinear Dynamics in a Complex Electrochemical System

Adrian Bîrzu [*]

Department of Chemistry, "Al.I. Cuza" University Iasi, 11 Carol I Bd, Iasi 700506, Romania

Abstract: This paper aims to offer a concise view of the nonlinear dynamics in electrochemical systems. Particular examples will be given using a model that qualitatively describes the anodic metal electrodissolution. Among the typical nonlinear behaviors exhibited by this system are bistable front propagation, periodic oscillations, standing waves, rotating pulses and chaotic dynamics.

Keywords: Nonlinear electrochemical systems; Bistability; Excitability; Oscillations; Chaotic dynamics.

Introduction

In order to observe typical nonlinear behaviors in a dynamical system, two conditions has to be fulfilled:[1]

- the system is characterized by nonlinear dynamical equations;
- the system is maintained far from equilibrium.

In case of a chemically reacting system, it's sometimes difficult to satisfy both conditions. However, electrochemical systems possess intrinsic properties that make them ideal candidates for the study of nonlinear

[*] Dr. Adrian Bîrzu, tel: +40 232 201344, fax: +40 232 201313, e-mail: abirzu@uaic.ro

dynamic properties.[2,3] This is the main reason why the nonlinearity in chemical systems started to be a hot topic of research just in seventies of the last century, while experimental studies regarding nonlinear electrochemical systems starts from 19th century. Still, the development of theoretical knowledge was necessary to perform systematic studies in both cases.[4,5]

A dynamical system whose properties are the same irrespective of the spatial coordinates is called point-like, or lumped parameter system.[4] Usually, the evolution of such a system is characterized by a small number of dynamical variables that are functions of time. The opposite is a spatially distributed or distributed parameter system,[4] whose dynamical variables are function of time and space. Most of the dynamical studies involving electrochemical systems were focused on point like systems, because of the theoretical and experimental complexity of distributed systems. Just after 1995, the works of Krischer boosted fruitful studies of spatially distributed nonlinear electrochemical systems.[2,3]

The present work belongs to the above mentioned field. The model employed by us describes in a qualitative fashion the anodic electrodissiolution of a metal in acidic solutions.[6] This model exhibits extremely rich dynamics, ranging from bistability, excitability, complex periodic oscillations to chaos.[6-10]

The model

Under potentiostatic control, metals can exhibit active – passive transition. This will lead to the onset of a Negative Differential Resistance (NDR) region in the current – potential characteristic. We modeled this property using a smoothed Heaviside function:

$$i_{\text{reac}} = \frac{A}{e^{-\alpha\left(-\phi_{\text{DL}}+V_{\text{f}}\left(\left[\text{H}^{+}_{\text{WE}}\right]\right)\right)}+1} \tag{1}$$

where i_{reac} is the density of the reaction current, A and α are constants, ϕ_{DL} is the drop of potential over the double layer in front of the working electrode (WE) and V_{f} is the active-passive transition potential, called also the Flade potential. This depends on the proton concentration in front of the WE,

$$V_{\text{f}} = F_1 + F_2 \log\left(\left[\text{H}^{+}_{\text{WE}}\right]\right) \tag{2}$$

At the WE, the charge balance equation is satisfied:

$$\sigma \left.\frac{\phi}{z}\right|_{\text{WE}} = -i_{\text{cap}} - i_{\text{reac}} = C_{\text{DL}} \left.\frac{\phi}{t}\right|_{\text{WE}} - i_{\text{reac}} \tag{3}$$

where σ is electrolyte conductivity, $\left.\frac{\partial\phi}{\partial z}\right|_{\text{WE}}$ is the vertical component of the potential gradient in front of the WE (see Figure 1, for the geometry of the electrochemical cell), and C_{DL} is the specific capacitance of the electrical double layer in front of the WE.

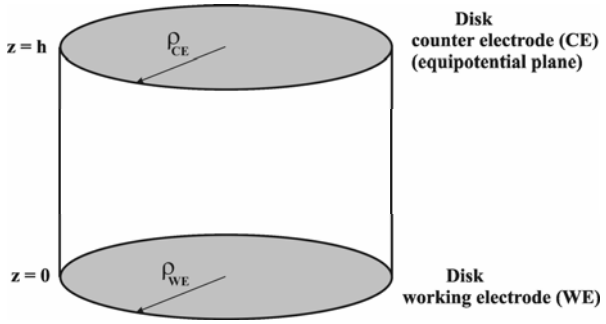

Figure 1. The geometry of the electrochemical cell.

This equation acts as a time dependent boundary condition at the WE. The concentration of protons in the bulk is supposed to be constant, while it has a linear variation in the diffusion layer in front of the WE. The

concentration changes in this layer because of diffusion and migration,

$$\frac{\left[\mathrm{H}^{+}_{\mathrm{WE}}\right]}{t} = \frac{2D\left(\left[\mathrm{H}^{+}_{\mathrm{bulk}}\right]-\left[\mathrm{H}^{+}_{\mathrm{WE}}\right]\right)}{\delta^2} + \frac{2\mu F\left[\mathrm{H}^{+}_{\mathrm{WE}}\right]}{\delta}\left.\frac{\phi}{z}\right|_{\mathrm{WE}} \tag{4}$$

Here, D is the diffusion coefficient, μ is the mobility, δ is the diffusion layer thickness and F is the Faraday constant.

In most of the experiments with metal electrodissolution, the conductivity of the electrolyte is high enough, and the electrolyte can be supposed to be electroneutral. Consequently, in the electrolyte the Laplace equation is satisfied:

$$\nabla^2\phi = \frac{\partial^2\phi}{\partial\rho^2} + \frac{1}{\rho}\frac{\partial\phi}{\partial\rho} + \frac{1}{\rho^2}\frac{\partial^2\phi}{\partial\theta^2} + \frac{\partial^2\phi}{\partial z^2} = 0 \tag{5}$$

where the position in the cell was described using the cylindrical coordinates (ρ,θ,z). The lateral cell boundary is supposed to be insulating,

$$\left.\frac{\partial\phi}{\partial\rho}\right|_{\rho=\rho_{\mathrm{WE}}} = 0 \tag{6}$$

The upper plane of the disk is supposed to be equipotential, according to the potentiostatic control,

$$\left.\phi\right|_{z=h} = -E_{\mathrm{apl}} \tag{7}$$

where E_{apl} is the applied voltage. The drop of potential across the double layer in front of the WE is related to the potential in the electrolyte, in front of the WE:

$$\phi_{\mathrm{DL}} = -\left.\phi\right|_{\mathrm{WE}} \tag{8}$$

The cell geometry depicted in Figure 1 tends to favour spatially uniform states for the WE. In such a situation, the partial differential equations (3) and (4) reduce to ordinary differential equations:

$$\begin{cases} C_{\mathrm{DL}} \dfrac{\mathrm{d}\phi_{\mathrm{DL}}}{\mathrm{d}t} = -\dfrac{A}{\mathrm{e}^{-\alpha\left(-\phi_{\mathrm{DL}}+V_{\mathrm{f}}\left(\left[\mathrm{H}^{+}_{\mathrm{WE}}\right]\right)\right)}+1} + \sigma\dfrac{E_{\mathrm{apl}}-\phi_{\mathrm{DL}}}{h} \\ \dfrac{\mathrm{d}\left[\mathrm{H}^{+}_{\mathrm{WE}}\right]}{\mathrm{d}t} = \dfrac{2D\left(\left[\mathrm{H}^{+}_{\mathrm{bulk}}\right]-\left[\mathrm{H}^{+}_{\mathrm{WE}}\right]\right)}{\delta^2} - \dfrac{2\mu F\left[\mathrm{H}^{+}_{\mathrm{WE}}\right]}{\delta}\dfrac{E_{\mathrm{apl}}-\phi_{\mathrm{DL}}}{h} \end{cases} \quad (10)$$

Being a two-variable autonomous system, it can exhibit just simple dynamical behaviors, like monostability (excitable or not), bistability and periodic oscillations.[4] On the other hand, considering the spatial extension makes the system to be characterized by an infinite number of degrees of freedom, allowing a rich variety of dynamical behaviors which includes spatio-temporal chaos.[6-9] This model is qualitative, and aims to capture just the main features of the metal electrodissolution processes in acidic solutions, being independent on a particular experimental system of this kind.

Results and discussions

1. Numerical aspects

For the bistable and excitable dynamics, the ordinary differential equations (10) with appropriate initial conditions were integrated using LSODE package of Hindmarsh.[11] In the case of spatio-temporal chaos, the partial differential equation (5) with time dependent boundary conditions (3) and (4) has to be solved. The Laplace's equation has been solved using a second-order finite difference method on a cylindrical grid, with 61x60x16 grid points in radial, angular and vertical direction respectively, by employing the ma48 subroutine package from HSL 2002 library.[12] This package takes advantage of matrix sparsity. Solving this problem using an

usual algorithm, like Gauss-Jordan or LU decomposition would be prohibitive:

- in terms of necessary RAM memory: for example, for the spatial resolution used here, which is average, 3.4 GB of RAM memory would be necessary just to store the coefficient matrix;

- in terms of CPU time: for example, doubling the spatial resolution would result in an increase of CPU time by $8^3 = 512$ times. The time dependent boundary conditions were integrated using a fourth-order Runge-Kutta method.[13] The autocorrelation function was computed using SANTIS data analysis software,[14] while the power spectrum was computed using a FFT algorithm.[13]

2. Bistable and excitable dynamics

Bistability is a typical feature of the N-shaped NDR electrochemical systems: the system possesses three stationary states, one unstable and two stable.

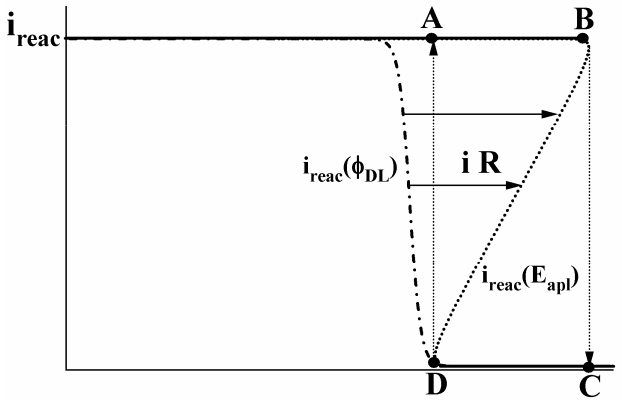

Figure 2. Current – voltage characteristic for an active – passive transition.

The onset of bistability can be explained based on the plot from Figure 2. The branches AB (high current, active state) and CD (low current,

passive state) are stable. The transition between them corresponds to a negative differential resistance region (dash-dotted line). When the characteristic is plotted function of the applied voltage, then the Ohmic drop in the electrolyte has to be considered, according to the equation

$$E_{\text{apl}} = \phi_{\text{DL}} + iR$$

Consequently, the line will be shifted proportionally to the value of the current, as total resistance of the electrolyte, R, is constant (dotted line). As a result, a hysteretic behavior, which is a fingerprint of the nonlinearity, appears: increasing the applied voltage, from the active state B the system will jump to C, in a passive state. The opposite transition occurs from D to A.

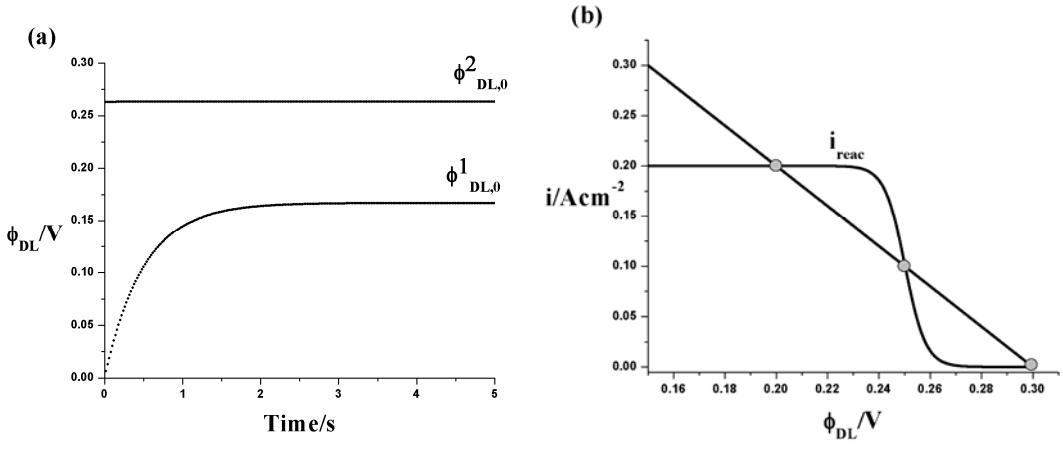

Figure 3. Bistability. a. Time dependence of the double layer potential for two different initial conditions: (0.2632;1.01) and (0;1.01) respectively. E_{apl} = 0.267 V . b. Reaction current and the load line. The parameters are the same as for (a), excepting E_{apl} = 0.3 V .

Figure 3a displays bistable behavior in the point like system described

by equations (10): depending on the initial condition, the system goes either to an active $\left(\phi_{DL} = \phi^{1}_{DL,0}\right)$ or to a passive $\left(\phi_{DL} = \phi^{2}_{DL,0}\right)$ stationary state. The parameter values are $C_{DL} = 1\,\mathrm{F \cdot cm^{-2}}$, $E_{apl} = 0.267\,\mathrm{V}$, $h = 0.2\,\mathrm{cm}$, $\sigma = 0.4\,\Omega^{-1} \cdot \mathrm{cm^{-1}}$, $A = 0.2\,\mathrm{A \cdot cm^{-2}}$, $\alpha = 250$, $F_1 = 0.25\,\mathrm{V}$, $F_2 = 0.06\,\mathrm{V}$, $D = 5 \cdot 10^{-6}\,\mathrm{cm^2 \cdot s^{-1}}$, $\delta = 0.01\,\mathrm{cm}$, $\mu = 5 \cdot 10^{-3}\,\mathrm{cm^2 \cdot V^{-1} \cdot s^{-1}}$, $\left[\mathrm{H^+_{bulk}}\right] = 1.2\,\mathrm{M}$. In a spatially distributed system, bistability can lead to a typical nonlinear process, namely the front propagation.[6,8] According to the first equation 10, stationary states appear at the intersection between the reaction current and the load line. In this case, three stationary states exist; while the extreme ones are stable, corresponding to those depicted in Figure 3a, the intermediate one, residing on a branch with negative slope of the characteristic is unstable.[2,3] From Figure 3b becomes also clear why the bistability occurs for intermediate values of conductivity; this condition derives from the condition to have three intersection points. If the conductivity is too low or too high, the system displays monostability, i. e., it presents a single stable stationary state.

Excitability is widely spread for example in biological systems and is responsible for example for impulse propagation along nerves. Figure 4 displays typical excitable dynamics: while the excitable stationary state is stable (continuous line in Figure 4a), a small perturbation drives the system away from this state, and then the system returns – here oscillatory, because the stationary state is a stable focus – to the initial state. An important property of the excitable systems is the refractory time: a given time after the perturbation, the system is insensitive to a new perturbation. Figure 4b shows the large excurse followed by the phase space trajectory before returning to the stable stationary state. In spatially extended systems,

excitable dynamics can lead to complex dynamics, including excitable pulse propagation, spiral wave dynamics,[10] and spiral chaos.

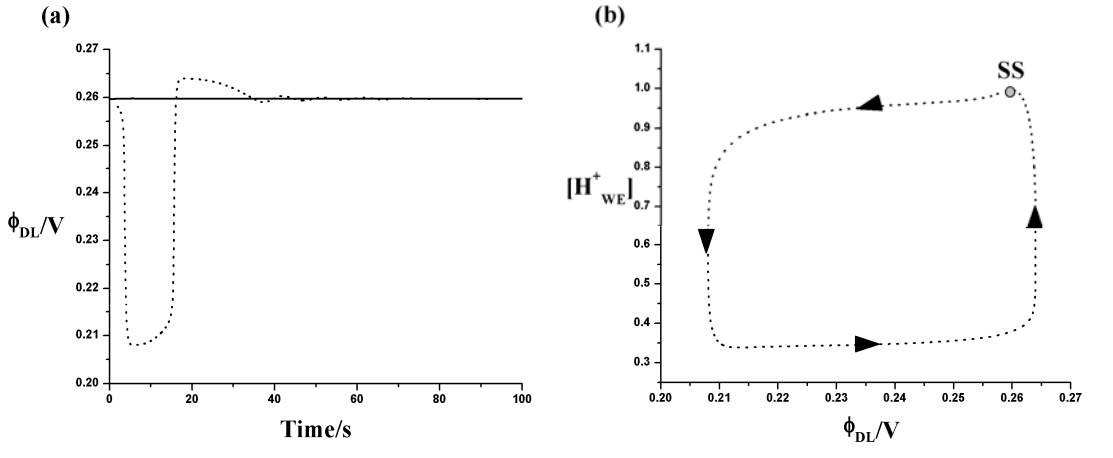

Figure 4. Excitable dynamics. Parameter values are the same as in Figure 3, excepting $\sigma = 0.714\ \Omega^{-1} \cdot \mathrm{cm}^{-1}$ and $E_{\mathrm{apl}} = 0.264$ V. Excitable stationary state (0.2597;0.9904), and perturbation (0.26;1). a. Stationary state (continuous line) and response to perturbation (dotted line); b. Response to perturbation, in the phase space.

3. Spatio-temporal chaos

In spatially extended nonlinear systems, the concept of coupling is of paramount importance:[2,3] frequently, two different locations in the system do not act independently, but are coupled, the coupling being characterized by range and intensity. In an electrochemical system, coupling occurs through the electrical field, and is nonlocal in nature. For the cell depicted in fig. 1, the coupling range depends on the geometric ratio h/ρ_{WE}; the smaller is this ratio, the shorter range is the coupling. The coupling strength is proportional to the electrolyte conductivity. For an autonomous system described by two variables, the only accessible dynamics is stationary or

periodic.[4] However, a spatially extended system is characterized by an infinity of degrees of freedom and even a two-variable system can display much more complicate dynamics, including spatio-temporal chaos.[15,16] For our system, when the geometric aspect ratio is much smaller than one, $h/\rho_{\mathrm{WE}} \ll 1$, and the conductivity is low, the correlation in time and space decreases until the system displays spatio-temporal chaos. The parameter values used in simulations are those for Figure 3, excepting $\sigma = 0.2\ \Omega^{-1}\cdot\mathrm{cm}^{-1}$, $F_2 = 12\ \mathrm{V}$, $A = 0.02\ \mathrm{A}\cdot\mathrm{cm}^{-2}$, and $E_{\mathrm{apl}} = 0.27\ \mathrm{V}$. Geometrical parameter values are $h = 2\ \mathrm{cm}$, and the circumference of the cell is $l_{\mathrm{C}} = 150\ \mathrm{cm}$. The initial condition at the WE is spatially uniform, equal to $\left(\phi_{\mathrm{DL}}^{0}, \left[\mathrm{H}_{\mathrm{WE}}^{+}\right]^{0}\right) = (0.26; 0.9929)$.

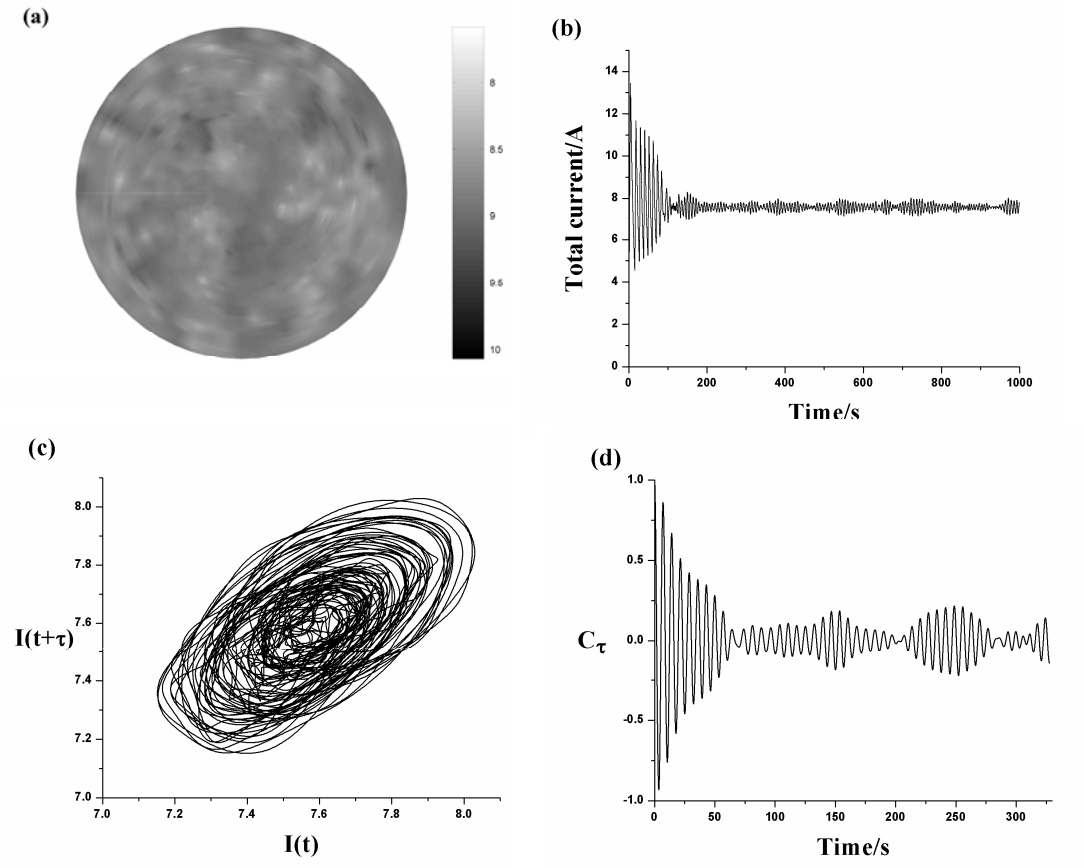

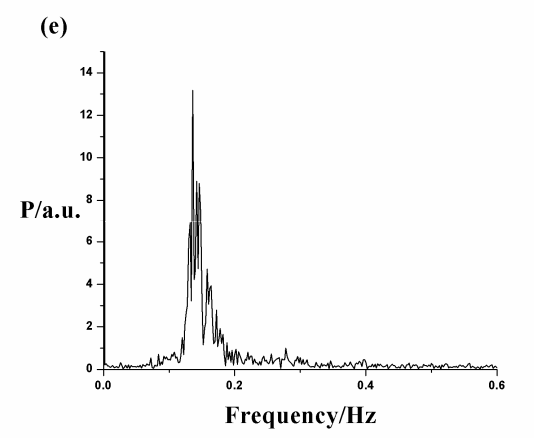

Figure 5. Spatio-temporal chaotic dynamics. a. Grayscale contourplot representation of the double layer potential distribution across the WE at the end of the integration time. b. Time evolution of the total current; c. Phase portrait; d. Autocorrelation function; e. Power spectrum.

Figure 5a displays $\phi_{\mathrm{DL}}(\rho,\theta)$ across the WE, at a given moment, for a fully developed turbulent state. In this representation, white corresponds to low ϕ_{DL} values (active state), while black corresponds to passive state. Inspecting the plot is visible that the correlation in space tends to zero, and two different locations on the surface of the WE act independently. On the other hand, Figures 5b and 5d illustrate the loss of temporal correlation. The signal looks more regular in this plot for the first 100 seconds, because during this time only the radial symmetry is broken, the angular one being preserved.[15] In order to plot the phase portrait from Figure 5c, the time delay method was used, with a delay of 100 points (1 second). The phase portrait confirms the chaotic character of the dynamics: the phase space trajectories cover in a dense fashion a given region of the phase space,

giving rise to a strange attractor.[4] The autocorrelation function decreases in an oscillatory manner to 0, meaning the dynamics is chaotic. Finally, Figure 5e unveils an intriguing property of this system: the chaotic dynamics is characterized by a quite narrow band in the power spectrum, corresponding to a frequency (0.136 Hz) which is much lower than the natural frequency of the point-like system with the same parameter values (0.584 Hz). The largest Lyapunov exponent calculated for the total current time series is equal to 0.116, confirming once more the chaotic dynamics.[17]

Conclusions

Electrochemical systems prove to be ideal candidates for the study of nonlinear properties. The employed model describes qualitatively the anodic electrodissolution of metals; these systems were found often experimentally to exhibit typical nonlinear processes.[2,3] We studied (a) the point-like system, in particular bistability and excitability, and (b) the spatially extended system, to explore some properties of the spatio-temporal chaotic dynamics.

The mechanism for the onset of bistability is presented in detail. Then, the spatio-temporal chaos is studied, using standard tools of nonlinear time series analysis, like phase portrait, autocorrelation function, power spectrum and the largest Lyapunov exponent. The future studies centered on this system will focus on its bifurcation properties, both for point-like and spatially extended cases.

Acknowledgements

The author acknowledges support from the CNCSIS grant 2219/2008.

References

1. Bourceanu, G. and Bîrzu, A., *"Termodinamica evoluţiei şi dinamică neliniară"*, MatrixROM: Bucureşti, 2003.
2. Krischer, K., in *"Modern Aspects of Electrochemistry"*, Conway, B. E., Bockris J. O'M., and White, R. E., Eds., Kluwer Academic/Plenum: New York, 1999, vol. **32**, p. 1.
3. Krischer, K., in *"Advances in Electrochemical Science and Engineering"*, Alkire R. C. and Kolb, D. M., Eds., VCH: Weinheim, 2003, vol. **8**, p. 89.
4. Strogatz, S. H., *"Nonlinear Dynamics and Chaos"*, Addison Wesley: Reading, 1994.
5. Kantz, H. and Schreiber, T., *"Nonlinear time series analysis"*, Cambridge University Press: Cambridge, 1997.
6. Bîrzu, A., Green, B. J., Otterstedt, R. D., Jaeger, N. I., and Hudson, J. L., *Phys. Chem. Chem. Phys.*, **2**, 2715 (2000).
7. Bîrzu, A., Green, B. J., Jaeger, N. I., and Hudson, J. L., *J. Electroanal. Chem.*, **504**, 126 (2001).
8. Bîrzu, A., Green, B. J., Otterstedt, R. D., Hudson, J. L., and Jaeger, N. I., *Z. Phys. Chem.*, **216**, 1 (2002).
9. Bîrzu, A., Plenge, F., Jaeger, N. I., Hudson, J. L., and Krischer, K., *J. Phys. Chem. B*, **107**, 5825 (2003).
10. Bîrzu, A., Plenge, F., Jaeger, N. I., Hudson, J. L., and Krischer, K., *Phys. Chem. Chem. Phys.*, **5**, 3724 (2003).
11. Radhakrishnan, K. and Hindmarsh, A. C., *Description and Use of LSODE, the Livermore Solver for Ordinary Differential Equations*, LLNL report UCRL-ID-113855, 1993.

12. *HSL 2002, A collection of Fortran codes for large scale scientific computation*, http://www.cse.scitech.ac.uk/nag/hsl/.
13. Press, W. H., Teukolsky, S. A., Vetterling, W. T., and Flannery, B. P., *"Numerical recipes in Fortran 77"*, Cambridge University Press: Cambridge, 1992.
14. Vandenhouten, R., *"SANTIS – a tool for signal analysis and time series processing"*, RWTH: Aachen, 1996.
15. Bîrzu, A. and Krischer, K., *Phys. Chem. Chem. Phys.*, **8**, 3659 (2006).
16. Bîrzu, A. and Krischer, K., *Z. Phys. Chem.*, **221**, 1245 (2007).
17. Wolf, A., Swift, J. B., Swinney, H. L., and Vastano, J. A., *Phys. D.*, **16**, 285 (1985).